ChemComm

RSC Publishing

COMMUNICATION

View Article Online
View Journal | View Issue

Cite this: *Chem. Commun.*, 2013, **49**, 3221

Received 16th January 2013,
Accepted 27th February 2013

DOI: 10.1039/c3cc41362d

www.rsc.org/chemcomm

Ultra-stable CdS incorporated Ti-MCM-48 mesoporous materials for efficient photocatalytic decomposition of water under visible light illumination†

Rui Peng,[a] Chia-Ming Wu,[a] Jonas Baltrusaitis,[b] Nada M. Dimitrijevic,[c] Tijana Rajh[c] and Ranjit T. Koodali*[a]

A RuO_2–CdS–Ti-MCM-48 mesoporous material has been prepared. This composite material generates hydrogen and oxygen in the absence of a Pt co-catalyst and most importantly photocorrosion of CdS is completely eliminated.

Photocatalytic cleavage of water has been acknowledged as a clean means to generate hydrogen and oxygen to alleviate the impact of fossil fuels and address global environmental issues. The photoelectrochemical splitting of water was originally realized by Fujishima and Honda under UV illumination.[1] Inspired by this work, extensive efforts have been devoted and a myriad of semiconductors have been explored.[2–4]

CdS has been explored extensively in photocatalysis.[5] However, a big drawback of CdS is its propensity to undergo photocorrosion.[6] Efforts to alleviate this include use of sulfides/sulfites as sacrificial electron donor/agents, deposition of noble metals, incorporation of CdS into porous materials and preparation of coupled semiconductors.[5,7,8] Confinement of CdS clusters in porous supports provides advantages such as: (i) high dispersion of the semiconductor material that affords several catalytic sites per nm,[2] (ii) enhanced stability towards photocorrosion since less surface area of CdS is exposed, and (iii) limiting the size of CdS due to quantum confinement that shifts the conduction band (c.b.) edge to more negative values. The small size of the semiconductor enables fast diffusion of charge-carriers to the surface active sites thus minimizing the volume recombination of these charge carriers in CdS clusters. Moreover, the host porous materials can also provide extra pathways for migration of photoinduced electrons and thus facilitate charge-carrier separation and further increase the photocatalytic efficiency. Another strategy to enhance the photocatalytic activity of CdS is to couple it with other semiconductors.[9–11]

We have previously reported that MCM-48, with its interpenetrating 3-D pores, favours mass transfer kinetics and high dispersion of CdS.[7] However the drawback was the lack of O_2 generation and loss of CdS due to photocorrosion. In this work, CdS was incorporated into Ti-MCM-48 and loaded with the RuO_2 co-catalyst[12–17] and we realize generation of both H_2 and O_2. The ESI† section contains details of the synthesis. Most importantly, our XPS results indicate *no loss* of *CdS* after the reaction and production of H_2 and O_2 is sustained.

CdS incorporated into mesoporous materials have been studied before,[8,18] but suffer from the following drawbacks: synthesis of mesoporous materials that are quite time-intensive (up to 7 days), and/or conducted at relatively high temperatures, use of corrosive sulfides as sacrificial agents, use of a Pt co-catalyst, very low H_2 yield and absence of O_2, lack of photostability studies, loss of CdS, and formation of CdO after the reaction. To the best of our knowledge, this is the first report on CdS incorporated into mesoporous silica that demonstrates visible light: (i) generation of both H_2 and O_2 in the absence of the Pt co-catalyst, (ii) *no* photocorrosion of CdS even in the *absence* of sulfides or sulfites, and (iii) mild conditions for preparation of CdS–Ti-MCM-48 composites. Fig. 1 presents the low angle XRD patterns of all studied samples.

A characteristic Bragg reflection due to cubic $Ia\bar{3}d$ symmetry can be perceived in all samples. The strong peaks due to d_{211} and weak d_{220} reflections in the range of 2.5–3.5° demonstrate that the cubic phased mesopore structure was preserved after

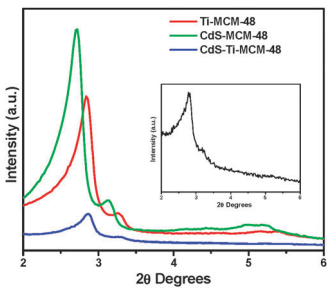

Fig. 1 Low angle XRD patterns of studied samples. The inset plot represents the RuO_2–CdS–Ti-MCM-48 sample.

[a] *Department of Chemistry, University of South Dakota, Vermillion, SD 57069, USA. E-mail: Ranjit.Koodali@usd.edu*
[b] *PhotoCatalytic Synthesis Group, University of Twente, The Netherlands*
[c] *Center for Nanoscale Materials, and Chemical Sciences and Engineering Division, Argonne National Laboratory, Argonne, Illinois 60439, USA*

† Electronic supplementary information (ESI) available. See DOI: 10.1039/c3cc41362d

incorporation of TiO_2, RuO_2, and CdS. Moreover, the peaks, due to d_{321}, d_{400}, d_{420}, and d_{332} in the interval of 4–6° indicate high ordered array of mesopores.[19] Compared to the Ti-MCM-48 sample, CdS–Ti-MCM-48 and RuO_2–CdS–Ti-MCM-48 exhibited less intense peaks. The decrease in peak intensity can be ascribed to the addition of CdS and/or RuO_2 species that cause the lack of the scattering contrast between the pores and pore walls. The high angle XRD patterns of the samples (Fig. S1, ESI†) show a broad peak at 2θ near 22.5° due to bulk silica. The absence of peaks due to TiO_2, RuO_2, and CdS suggests that these components are highly dispersed in MCM-48. In addition, it is possible that the extremely small size of these species precludes its detection limit of XRD. Nitrogen isotherms (Fig. S2a, ESI†) show a reversible isotherm of type IV indicating the mesoporous nature. The pore size distribution of all the studied samples exhibits a highly uniform material (Fig. S2b, ESI†). A summary of the textural properties of the samples is listed in Table S1 (ESI†).

UV-Vis diffuse reflectance spectroscopy (DRS) is useful in evaluating the local environment of Ti^{4+} and determining the particle size of CdS.

Fig. 2 shows the DRS spectra of all samples. In Ti-MCM-48, the strong absorption at ~210 nm is attributed to the ligand to metal charge transfer from O^{2-} to Ti^{4+} in tetrahedral coordination. A broad shoulder at ~270 nm indicates the presence of a fraction of Ti^{4+} in octahedral geometry. The absence of a peak near 330 nm suggests that no bulk TiO_2 is formed in Ti-MCM-48. Also, the absorption onsets of all Ti-MCM-48 samples are ~350 nm. This indicates that the Ti species are highly dispersed in MCM-48. Meanwhile, the position of adsorption onsets of CdS containing MCM-48 exhibits a significant blue shift (~500 nm) compared to bulk CdS (~600 nm). The blue shift in the CdS absorption onset is due to quantum confinement effects. The band gap energy of the CdS species in CdS-MCM-48 and RuO_2–CdS–Ti-MCM-48 is 2.46 eV and the particle size of CdS is estimated to be ~3.4 nm from the Brus equation.[20] Similarly, the band gap energy of CdS in CdS–Ti-MCM-48 is 2.43 eV, and the particle size of CdS is 3.6 nm. The particle size of CdS is larger than the size of mesopores in Si- and Ti-MCM-48 materials. It is well-documented that small CdS clusters can agglomerate in porous materials including MCM-48 due to quantum tunneling effects.[21] Nitrogen sorption (a decrease in pore volume from 0.76 to 0.66 cm^3 upon loading CdS) and DRS studies indicate that most of the CdS particles are embedded in the pores of MCM-48 while a small portion of CdS deposited on the external surface of MCM-48 cannot be completely eliminated. X-ray photoelectron spectroscopy (XPS) is a sensitive tool for investigating the surface chemical composition and oxidation state. The XPS plots (Fig. S3, ESI†) of CdS incorporated samples show peaks at 411.6 and 404.9 eV due to Cd $3d_{5/2}$ and $3d_{3/2}$ with a separation of 6.7 eV which is typical of CdS. The S^{2-} $2p_{1/2}$ and $2p_{3/2}$ peaks appear at 162.4 eV and 161.2 eV and support the formation of CdS. The ratio of S^{2-} to silica was determined to be 0.015 in the sample prior to photocatalytic reaction.

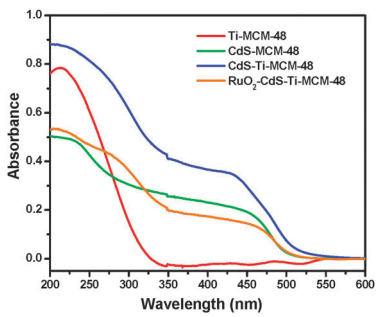

Fig. 2 Diffuse reflectance spectra of MCM-48 samples.

Table 1 Photocatalytic activities of MCM-48 materials

Sample	H_2 evolution rate (mmol h^{-1} $g_{catalyst}{}^{-1}$)	O_2 evolution rate (mmol h^{-1} $g_{catalyst}{}^{-1}$)	AQY[a]
Ti-MCM-48	0	0	0%
CdS-MCM-48	0.22	0	2.9%
CdS–Ti-MCM-48	2.73	0	36.3%
RuO_2–CdS–Ti-MCM-48	0.26	0.13	3.5%

[a] $\mathrm{AQY}(\%) = \dfrac{\text{the number of evolved } H_2 \text{ molecules} \times 2}{\text{the number of incident photons}} \times 100.$

The photocatalytic H_2 and/or O_2 evolution rate and the apparent quantum yield (AQY) are listed in Table 1. Ti-MCM-48 does not generate H_2 and O_2 under visible light. In contrast, all the CdS containing MCM-48 photocatalysts exhibit a significant amount of H_2. Compared to the H_2 production generated by the CdS-MCM-48 sample (0.22 mmol h^{-1} $g_{catalyst}{}^{-1}$), CdS–Ti-MCM-48 gives a higher H_2 evolution rate (2.73 mmol h^{-1} $g_{catalyst}{}^{-1}$). This remarkable increase in the photocatalytic activity is mainly due to the presence of well dispersed TiO_2 clusters that facilitate transfer of electrons from the c.b. of CdS to TiO_2 in CdS–Ti-MCM-48, thus minimizing electron–hole recombination. Also, the valence band (v.b.) edge of TiO_2 clusters is more positive than the v.b. of CdS and hence, holes in the v.b. of CdS cannot diffuse to the TiO_2 v.b. TEM images of CdS–Ti-MCM-48 and RuO_2–CdS–Ti-MCM-48 are shown in Fig. S4 and S5 (ESI†). In RuO_2–CdS–Ti-MCM-48, at low magnifications (Fig. S5a, ESI†), the cubic phase is seen along with some dark contrasts. At high magnifications (Fig. S5b and S5c, ESI†), one can see lattice fringes. Careful examination of the fringes indicates the presence of RuO_2 with a d_{200} spacing of 2.43 Å. In addition, lattice fringes due to CdS and TiO_2 are also seen with a d_{101} spacing of 3.13 Å and a d_{101} spacing of 3.54 Å, respectively. As stated previously, the particle size of CdS estimated from DRS studies is ~3.4 nm and the particle size of RuO_2 estimated from TEM studies is ~7.5 nm. The results obtained from Energy Dispersive X-ray Spectroscopic (EDS) studies are shown in Fig. S5d (ESI†), and the distribution of the various elements can be observed. In addition, EDS mapping results indicate the close contact of RuO_2 particles with CdS and TiO_2. The fairly high dispersion of titania in the silica support is also observed.

Interestingly, in RuO_2–CdS–Ti-MCM-48, the stoichiometric ratio of H_2 (1.56 mmol) and O_2 (0.75 mmol) was achieved by utilizing visible light in the presence of ethanol after 6 h of irradiation. Alcohols such as ethanol have been employed as sacrificial electron donors and higher H_2 yields have been observed since they can be easily photooxidized.[22] We have detected acetaldehyde in our experiments (but have not quantified them) since it is not the focus of our work. Surprisingly, in the presence of a hole transfer agent, *i.e.* in RuO_2–CdS–Ti-MCM-48, we also observe O_2. RuO_2 is a very active catalyst for O_2 evolution because of its low overpotential. In ethanolic solutions,

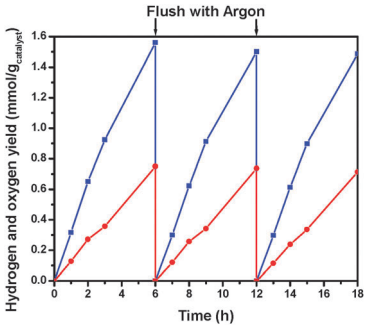

Fig. 3 Photocatalytic water splitting over RuO_2–CdS–Ti-MCM-48. Blue squares and red circles denote H_2 and O_2.

the holes produced in the v.b. of CdS can migrate to the surface of the photocatalyst and oxidize ethanol and may also be trapped at the surface by RuO_2 to produce O_2 and it seems that the trapping of the holes by RuO_2 is fairly efficient in our system since stoichiometric amounts of O_2 were formed. Thus, the presence of ethanol (sacrificial electron donor) and RuO_2 (low overpotential for O_2 generation) help in the formation of both hydrogen and oxygen. In the presence of pure water under identical conditions, RuO_2–CdS–Ti-MCM-48 forms stoichiometric amounts of H_2 (0.72 mmol $g_{catalyst}^{-1}$) and O_2 (0.35 mmol $g_{catalyst}^{-1}$) after 6 h of irradiation indicating the role of RuO_2 in generating O_2 but with lower yields as expected as shown in Fig. S6 (ESI†).

To investigate the stability of RuO_2–CdS–Ti-MCM-48, recycling studies were carried out. Fig. 3 shows the photocatalytic H_2 and O_2 rate of RuO_2–CdS–Ti-MCM-48 in ethanol. The results indicate that RuO_2–CdS–Ti-MCM-48 is extremely robust and its photocatalytic activity is sustainable. However, RuO_2–CdS–Ti-MCM-48 shows a significant decrease in the H_2 evolution rate (0.26 mmol h^{-1} $g_{catalyst}^{-1}$) compared to CdS–Ti-MCM-48. The decrease in H_2 yield is probably due to RuO_2 species that also act as recombination centres of the photogenerated electron–hole pairs.[12] Also, the loading sequence of RuO_2 is prior to CdS into Ti-MCM-48, and thus, the RuO_2 clusters may preclude intimate contact between CdS and TiO_2. In addition, the higher absorbance of CdS–Ti-MCM-48 in comparison to RuO_2–CdS–Ti-MCM-48 may also be a factor responsible for enhanced hydrogen production in CdS–Ti-MCM-48. In order to elucidate the photoinduced charge carrier transfer pathways in CdS–Ti-MCM-48 samples, the electron paramagnetic resonance (EPR) study was carried out. Irradiation of CdS by visible light leads to the production of electron–hole pairs. As suggested previously, electrons promoted to the c.b. in CdS can be injected into TiO_2. EPR signals were monitored by irradiating the sample with visible light (cut off filter 400 nm) in the presence of glycerol. The EPR spectrum of CdS–Ti-MCM-48 (Fig. S7a, ESI†) indicates the formation of Ti^{3+} ($g_\perp$ = 1.958 and $g_\parallel$ = 1.920), which is evidence for electron transfer from CdS to TiO_2. A strong signal near g = 2.004 is due to organic radicals formed by the reaction of photogenerated holes with glycerol.[23] A stronger Ti^{3+} peak is found for CdS–Ti-MCM-48 (Fig. S7a, ESI†) compared to that for the RuO_2 containing sample as seen in the EPR plot (Fig. S7b, ESI†). Hence, efficient transfer of electrons from CdS to TiO_2 is prevented and H_2 production diminished. Most importantly, XPS studies of CdS–Ti-MCM-48 samples do not show any loss of CdS after the photocatalytic reaction (the ratio of S^{2-} to silica in the spent catalyst remains to be 0.015) even though the reaction was carried out in the absence of sulfides and sulfites as sacrificial agents. Also, in the XPS plots (Fig. S8, ESI†) of the spent catalysts, CdS shows peaks at 411.6 and 404.9 eV due to Cd $3d_{5/2}$ and $3d_{3/2}$ and S^{2-} $2p_{1/2}$ and $2p_{3/2}$ peaks at 162.4 eV and 161.2 eV that indicate the retention of CdS. The intensities of Cd and S in the fresh and spent samples remain virtually unchanged indicating the high stability of CdS after encapsulation in the MCM-48 matrix. Our AAS results also confirm the retention of CdS in RuO_2–CdS–Ti-MCM-48 after long-term photocatalytic reaction and indicate no loss of CdS. The generation of O_2 also indicates that the holes produced in the v.b. of CdS do not cause photocorrosion and that oxidation of water occurs as suggested previously.[17]

Thanks are due to NSF–CHE-0722632, NSF–EPS-0903804, DE–EE0000270, and SD NASA-EPSCOR NNX12AB17G. The work at the Center for Nanoscale Materials was supported by the U.S. DOE, under contract DE-AC02-06CH11357.

Notes and references

1 A. Fujishima and K. Honda, *Nature*, 1972, **238**, 37–38.
2 A. Kudo and Y. Miseki, *Chem. Soc. Rev.*, 2009, **38**, 253–278.
3 X. Chen, S. Shen, L. Guo and S. S. Mao, *Chem. Rev.*, 2010, **110**, 6503–6570.
4 M. Ashokkumar, *Int. J. Hydrogen Energy*, 1998, **23**, 427–438.
5 M. D. Hernandez-Alonso, F. Fresno, S. Suarez and J. M. Coronado, *Energy Environ. Sci.*, 2009, **2**, 1231–1257.
6 T. Inoue, T. Watanabe, A. Fujishima, K.-i. Honda and K. Kohayakawa, *J. Electrochem. Soc.*, 1977, **124**, 719–722.
7 R. Peng, D. Zhao, J. Baltrusaitis, C.-M. Wu and R. T. Koodali, *RSC Adv.*, 2012, **2**, 5754–5767.
8 S. Y. Ryu, W. Balcerski, T. K. Lee and M. R. Hoffmann, *J. Phys. Chem. C*, 2007, **111**, 18195–18203.
9 Y. Chen, L. Wang, G. Lu, X. Yao and L. Guo, *J. Mater. Chem.*, 2011, **21**, 5134–5141.
10 T. Kida, G. Guan, Y. Minami, T. Ma and A. Yoshida, *J. Mater. Chem.*, 2003, **13**, 1186–1191.
11 H. Yan, J. Yang, G. Ma, G. Wu, X. Zong, Z. Lei, J. Shi and C. Li, *J. Catal.*, 2009, **266**, 165–168.
12 D. Duonghong, E. Borgarello and M. Graetzel, *J. Am. Chem. Soc.*, 1981, **103**, 4685–4690.
13 H. Kato, K. Asakura and A. Kudo, *J. Am. Chem. Soc.*, 2003, **125**, 3082–3089.
14 A. Iwase, H. Kato and A. Kudo, *Chem. Lett.*, 2005, **34**, 946–947.
15 M. Hara, C. C. Waraksa, J. T. Lean, B. A. Lewis and T. E. Mallouk, *J. Phys. Chem. A*, 2000, **104**, 5275–5280.
16 A. Ishikawa, T. Takata, J. N. Kondo, M. Hara, H. Kobayashi and K. Domen, *J. Am. Chem. Soc.*, 2002, **124**, 13547–13553.
17 K. Kalyanasundaram, E. Borgarello, D. Duonghong and M. Grätzel, *Angew. Chem., Int. Ed. Engl.*, 1981, **20**, 987–988.
18 T. Hirai, H. Okubo and I. Komasawa, *J. Phys. Chem. B*, 1999, **103**, 4228–4230.
19 B. Boote, H. Subramanian and K. T. Ranjit, *Chem. Commun.*, 2007, 4543–4545.
20 M. L. Steigerwald and L. E. Brus, *Annu. Rev. Mater. Sci.*, 1989, **19**, 471–495.
21 N. Herron, Y. Wang, M. M. Eddy, G. D. Stucky, D. E. Cox, K. Moller and T. Bein, *J. Am. Chem. Soc.*, 1989, **111**, 530–540.
22 U. Pal, S. Ghosh and D. Chatterjee, *Transition Met. Chem.*, 2012, **37**, 93–96.
23 R. Peng, D. Zhao, N. M. Dimitrijevic, T. Rajh and R. T. Koodali, *J. Phys. Chem. C*, 2012, **116**, 1605–1613.